J Mater Sci **(2024) 59:11278–11287**

Review

Review: pure, amorphous iron

H. K. D. H. Bhadeshia[1,*]

[1] *School of Materials Science and Engineering, Queen Mary University of London, Mile End Road, London, UK*

Received: 17 April 2024

Accepted: 4 June 2024

ABSTRACT

This is a review of glassy iron in its pure form, written in honour of Professor Kamanio Chattopadhyay's distinguished career, particularly with respect to highly metastable materials. The review covers the difficulty in obtaining amorphous iron, the clever experiments that have produced small particles or thin films of glassy iron, together with models that estimate the process parameters and many other features of disorder. Magnetic properties are highlighted though not fully understood.

Introduction

Professor Kamanio Chattopadhyay was creating knowledge at least two years before I took up doctoral research. His first paper in 1974, dealt with the structure of a eutectic alloy solidified over a heat pipe that he constructed himself (Fig. 1). The pipe has a chilling effect on any hot object that it comes into contact with; significantly, it is able to mitigate any unintended temperature excursion, such as might follow recalescence during solidification. The equipment therefore enabled large undercoolings to be achieved below the equilibrium freezing temperature [1].

That study was followed up a couple of years later, with publications on splat cooling experiments [4] and vapour deposition, aimed again at achieving greater undercoolings and extending the range of solubility of the nickel in aluminium, beyond that permitted by equilibrium. These were the heady days of battling thermodynamic constraints. The vapour deposited samples revealed, for the first time, multiple twinned particles in aluminium alloys, particles that were not too stable when subjected to examination in an 80 kV beam of electrons [1].

There was a brief excursion into the rapid cooling of a tool steel, ordered structures in a melt spun Fe–Si alloy, austenitic ductile iron, icosahedral $FeTi_2$, the iron–germanium system, but much of the subsequent work involved anything other than iron, or iron as a supplement. I felt therefore that Professor Chattopadhyay would be especially interested in an article on undercooled pure iron. He has written on the special behaviour of nanoparticles [5] and small particles [6]—glassy pure iron is limited to these length scales so I imagine that will intensify his interest. Pure amorphous iron is difficult to make in any sizeable quantities, so practical applications are unlikely—it nevertheless is a stimulating topic.

Handling Editor: Chandra Tiwary.

Address correspondence to E-mail: hkdb@qmul.ac.uk

Springer

https://doi.org/10.1007/s10853-024-09864-2

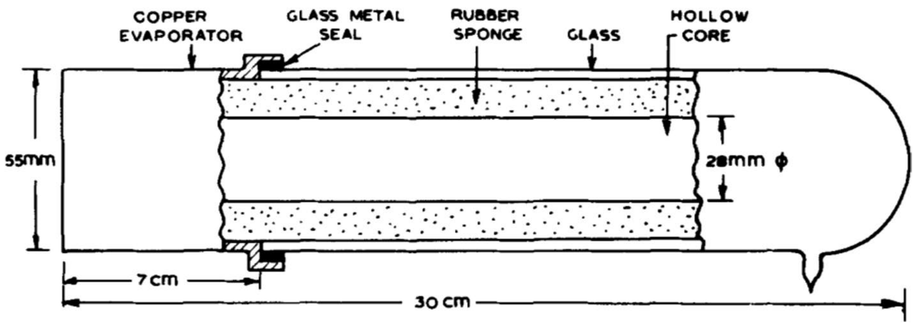

Figure 1 Original diagram of the heat pipe, 'a versatile heat transfer device', constructed for the experiments on an aluminium–copper eutectic. Its assembly involved some scavenging of a junk yard to harvest bits and pieces needed to build a respectable device [2]. Image from Chattopadhyay and Ramachandrarao [3] reproduced with permission of Elsevier.

Pure iron prefers to crystallise so to induce it into an amorphous solid necessitates cooling rates that we shall see are unachievable in practice. It is possible to precipitate slightly impure amorphous iron particles that are tiny, or films that are thin. Calculations that are revealing not only of the atomic configuration of the disordered solid, but which explain its magnetic and other characteristics, are possible. The caveat is that they should verifiably demonstrate configurationally frozen disorder.

Pair correlation functions

Any simulation of the atomic structure of amorphous iron must reproduce the experimental function describing the distribution of distances between a reference atom and another, in a given volume; it must also achieve a packing fraction that is close to the crystalline state [7]. If a reference atom sits at the origin $r = 0$, the pair correlation function $g\{r\}$ gives the probability $g\{r\}4\pi r^2\,\mathrm{d}r$ for another atom to be located at a distance r and $r + \mathrm{d}r$ [8]. The particular characteristic of this function for glassy iron is that the peak representing the second neighbours is split into two subsidiary maxima (Fig. 2). This splitting is a reflection of the atomic packing, best described in terms of Voronoi polyhedra and their connections. The stronger first sub-peak is attributed to polyhedra that share three atoms, the second where they share one atom and the dip in the middle to two-atom shared connections [9]. This splitting and the relative intensities of the two sub-peaks are regarded as an important validation of any model for the structure of amorphous iron when compared against experimental pair correlation functions. Thus, the random packing model originally representing the liquid state with the irregular and dense piling of spheres [10] fails in this respect. Other computations involving hard-sphere random-stacking fare better using specific criteria by which an amorphous cluster is built up from a seed onto which other atoms are attached in a stepwise manner [11, 12].

Simulations

A technique used to study the pair correlation functions of the different states of iron is a molecular dynamics simulation, which begins with a cubic arrangement of thousands of atoms. Furthermore, the notional assembly of atoms can be heated or cooled to

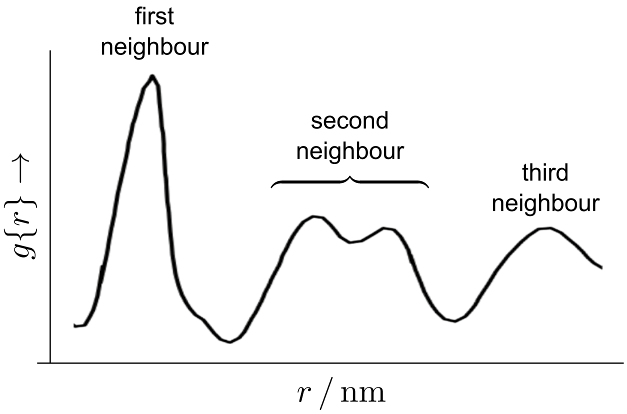

Figure 2 A pair correlation function for an iron-based metallic glass (Fe-B). Schematic diagram using selected data from [13]. The distance r is with respect to a reference atom and the vertical distance could be identified with the number of atoms per unit volume.

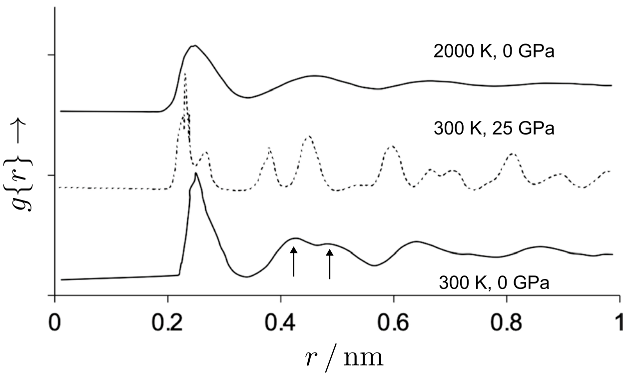

Figure 3 Pair correlation functions calculated using molecular dynamics simulations. The data for 2000 K are consistent with the liquid state of pure iron. The cooling rate $|\dot{T}|$ to 300 K was 10^{13} K s^{-1}. The arrows highlight the splitting of the second peak of the amorphous solid iron into two sub-peaks, to be compared against the function for the liquid where the second peak is a single maximum. The vertical origin of each set of data is arbitrary. Selected data from Mo et al. [14].

examine transitions. The real-time scales in such simulations are incredibly small so it is 'easy' to implement very large temperature changes. The molten assembly can be cooled so rapidly that the iron assumes a glassy state. Referring to Fig. 3, the calculated pair correlation function for the liquid generated at 2000 K and zero pressure shows a monotonic second peak, but on quenching to 300 K (zero pressure) the second neighbour peak splits into the sub-peaks characteristic of a glass.

Voronoi polyhedra can be expressed as $\langle n_3, n_4, n_5, n_6 \rangle$ where n_i refers to the number of i-edged faces. Simulations indicate that the distribution of atoms in amorphous iron, have polyhedra corresponding to $\langle 0,2,8,4 \rangle$, $\langle 0,3,6,4 \rangle$, $\langle 0,1,10,2 \rangle$ (Fig. 4) as the dominant construction blocks at ambient pressure [14], and some further data are shown in Table 1. Although some of these parameters can be similar for the amorphous and body-centred cubic forms of iron, the polyhedra in the former are likely to be distorted when compared against the regular ones in the crystalline form.

The simulations indicate that liquid iron would need to be quenched at $|\dot{T}| \approx 10^{13}$ K s^{-1} to solidify as a glass; this applies for pressures up to about 20 GPa. Pressures in excess of 20 GPa favour solidification to the crystalline state which has a smaller specific volume, giving rise to the peaks in the pair correlation function corresponding to the long-range periodicity of the structure [14]. It does not therefore seem possible to obtain sizeable chunks of *pure*, glassy iron.

The simulation cannot be replicated experimentally. But solids other than iron are known to undergo an amorphous to a denser amorphous state, apparently a first-order transformation induced by pressure. Low-density, amorphous ice when compressed at a pressure of about 10 atmospheres undergoes a sharp transition into another form of denser amorphous ice [15]. However, an amorphous→crystal transition under pressure is rare, but it does occur in silicon. High-density amorphous silicon crystallises into the presumably denser primitive hexagonal crystal structure at a pressure of about 14 GPa [16]. Similar transitions occur in amorphous Zr-based alloys [17] and amorphous selenium [18]. It is reasonable therefore, to accept the simulation result that at sufficiently large (hydrostatic) pressures, pure amorphous iron should crystallise.

From an experimental point of view, uniaxial compression of certain bulk metallic glass causes quasicrystals to germinate in shear bands, but this amorphous→ crystalline transformation has been

Figure 4 Dominant polyhedra (construction blocks) indicating the spatial distribution of atoms in amorphous iron.

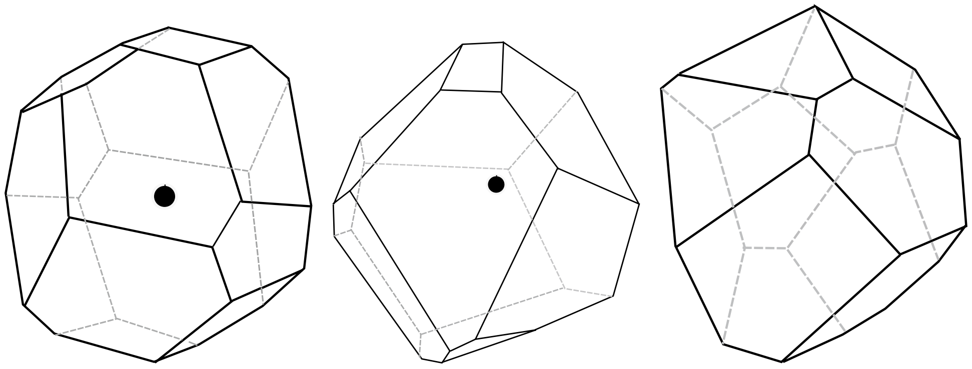
(a) (0,2,8,4) (b) (0,3,6,4) (c) 0,1,10,2

attributed to adiabatic heating due to the rate of deformation within those bands [19].

Another molecular dynamics simulation dealt with the quenching of liquid iron to 50 K; a completely amorphous state could be achieved when $|\dot{T}| \geq 10^{12.3}$ K s^{-1} [20]; this is consistent with the simulation in [14]. An examination of the atomic configurations indicated that a mixture of amorphous and α-iron crystals forms when $10^{11.98} \leq |\dot{T}| \leq 10^{12.3}$ K s^{-1} [1] and completely crystalline at any slower rates. A latent heat of transformation was observed only when the liquid crystallised. Interestingly, the cooling rate below which crystallisation sets in was estimated using independent homogeneous nucleation theory of the solidification of pure liquids [21] and agrees with the molecular dynamics simulations. Indeed, laser pulsing of pure iron is estimated to cool the surface at $|\dot{T}| \approx 10^{10}$ K s^{-1} but careful characterisation shows that the surface maintains crystallinity [22].

The molecular dynamics method [14] has been used to simulate the stress versus strain behaviour of pure iron metallic glass during uniaxial compression. Recalling that the method starts with a cubic arrangement of thousands of iron atoms, the box was compressed along one of its edges at a huge strain rate of 1×10^{10} s^{-1}. The yield strength was found to be very large at ≈ 5GPa, followed by a decrease in the stress required to propagate deformation to about 3.5 GPa, which remained about constant to a plastic strain of 0.5. However, the Young's modulus was recorded at just 90 GPa, which is much smaller than observed for iron-based bulk metallic glasses where it is in the range 192–213 GPa [23], close to the isotropic modulus for crystalline α-iron (210 GPa). Experimental stress–strain curves from uniaxial compression [23] do not show the maximum recorded in the simulation [14] (Fig. 5). It is probable that much of the simulated curve beyond yield is an artefact of the method.

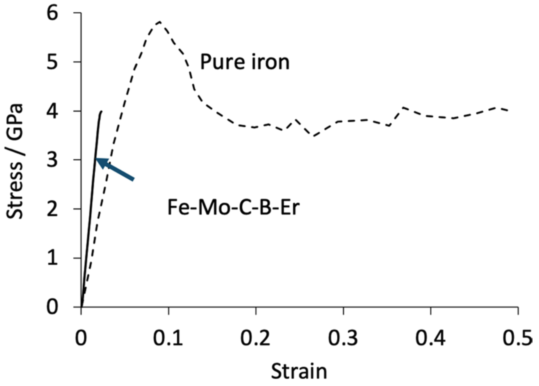

Figure 5 Metallic glasses uniaxially compressed. The curve with the larger modulus is from a bulk metallic glass of composition $Fe_{64.5}Mo_{14}C_{15}B_6Er_{0.5}$ [23], whereas the other one is a simulation of the uniaxial compression of amorphous pure iron using selected data from [14].

Experimental

An amorphous configuration of atoms in a solid alloy was first discovered in a gold–silicon alloy that was quenched from the liquid state [24]. That work stimulated an entire field of research on metallic glasses. Whereas iron has formed the basis of many metallic glasses, it is not feasible to obtain sizeable samples of *pure iron* in a glassy state.

However, small particles about 30 nm in size can be produced by subjecting an organometallic iron pentacarbonyl $Fe(CO)_5$ to intense ultrasound (20 kHz, 80 W cm^{-2}) that causes cavities in the liquid to form and collapse, processes associated with momentary high temperatures and pressures. The effective heating and cooling rates in such events exceed 10^9 K s^{-1}, resulting in the generation of amorphous iron particles that for further studies are filtered and washed in dry pentane while being kept away from oxygen and moisture [25, 26].

The particles are found to be ferromagnetic under ambient conditions with a magnetic moment of 1.7 μ_B per atom. The Curie temperature based on an assessment of a large quantity of data is ≈ 200 K [27]. This compares with 2.22μ_B per atom of crystalline α-iron, which has a much greater Curie temperature of 1042 K. The reduction in magnetic moment in the amorphous condition is probably because there is a distribution of exchange interactions that can lead to mixed magnetism, with confusion between ferro- and

---

[1] The coexistence of a two-phase mixture of crystal and glass obtained by quenching is difficult to understand unless the glass formed first and then partially crystallised. But if the crystals form directly from the liquid, then the liquid must be above its glass transition temperature so should completely solidify as crystals. Alternatively, the result could be an artefact of the small number of atoms (11,664) in the simulation.

antiferromagnetic coupling [28].[2] The amorphous iron cannot strictly be defined as ferromagnetic; because of the disorderly arrangement of atoms, the ferromagnetic axis 'wanders under the influence of the local balance of exchange', a phenomenon defined as *asperomagnetism* [29]. The evidence for the asperomagnetic state comes from calculations where the density of amorphous iron is unfortunately set at only 7.39 g cm^{-3} [30]. A value closer to 7.6 g cm^{-3} is realistic [31] and consistent with an atomic packing density of about 0.66 obtained in a model of the amorphous state that correctly reproduces the pair correlation function shown in Fig. 3 [7]. It may still therefore be reasonable to regard glassy iron with its large magnetic moment per atom as ferromagnetic below T_C [27, 31, 32].

Small amorphous iron particles can also be produced from a ferric chloride solution that is treated with NaBH$_4$ to reduce Fe^{3+} directly into iron [33], followed by magnetic separation and washing (Fig. 6). Ingenious experiments have been conducted on such particles using *in situ* heat treatment in a transmission electron microscope, to cause the particles to crystallise. The α-iron crystals that form on heating to 773 K grow rapidly until the amorphous phase is consumed in its entirety.

The crystallisation occurs in the range 585–775 K as the iron atoms become mobile. Nothing much is known about the evolution of the crystals within the amorphous matrix, or whether the particle surfaces play a significant role. For reasons that are not clear, small particles (≈ 200nm) crystallise at a higher temperature during continuous heating, all other things being equal [34], with transformation monitored using differential scanning calorimetry. The amorphous nanoparticles are magnetically soft (narrow hysteresis loop), so much so that the magnetic coercivity is close to zero at 300 K; it is only 190 Oersteds at 5 K but even this might be an artefact of the rate of the experiment (Fig. 7) [26]. The nanoparticles are unlikely to contain domain boundaries, so the magnetic softness is because there is no favoured direction along which the magnetic moments would prefer to be oriented [35], unlike the case for α-crystals.

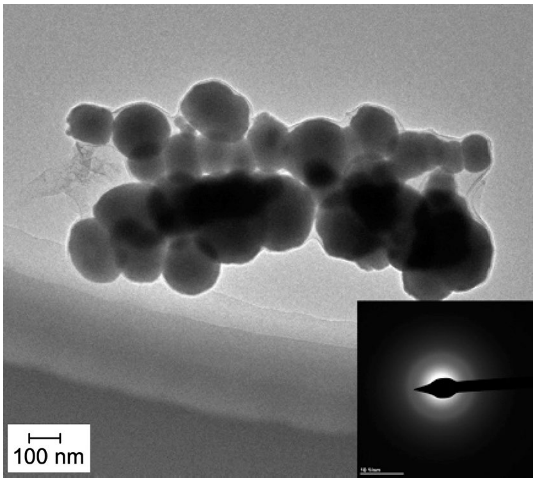

Figure 6 Amorphous iron particles obtained from a solution by the chemical reduction of Fe^{3+}. The diffuse electron diffraction pattern is consistent with an amorphous state. Image adapted from Falqui et al. [33] under the CC BY 4.0 licence, https://creativecommons.org/licenses/by/4.0/.

The presence of carbon in otherwise pure iron makes it easier to obtain the glassy state. A steel containing ≈ 4.3C wt% displayed substantial quantities of glass that could then be induced to crystallise on heating [36]. This is relevant to the amorphous iron produced using the pentacarbonyl method, because this iron is found to contain up to 3C wt% and up to 1 wt% of oxygen, perhaps from the pentane used to wash the reactive powder after synthesis [26, 37]. With a different preparation method involving the pentacarbonyl, about 2.6 wt% of carbon has been reported within the amorphous iron [38]. When such particles are heated, they crystallise into a mixture of cementite and α-iron [39]. Films 1–2μm thick of amorphous iron containing between 20–65C at.% can be made by sputtering [40]; these are much thicker than achieved for pure iron in the amorphous state (Sect. 7), confirming the role of carbon in stabilising the state.

Colloidal suspensions of amorphous iron

Dispersions of iron particles can be produced by heating Fe(CO)$_5$ to ≈ 150 °C in dilute solutions of polymers in an oxygen-free environment [41]. Particles smaller than ≈ 10 nm tend to be amorphous and some of the larger particles can contain amorphous cores surrounded by crystalline α-iron. They are magnetically single domain, with the magnetic moments within each particle aligned at ambient temperature. However, in a collection of

---

[2] When the wave functions of two atoms overlap, the electrons can to some extent be associated with either atom. The electrons therefore exchange roles and interact, with some correlation between their spins, which can lead to parallel or antiparallel alignment. Therefore, a distribution of spacing between atoms, as in an amorphous solid, would lead to a corresponding distribution in the magnitude of the exchange interaction. It is reasonable to ask why liquids, which have a density similar to amorphous solids, never exhibit ferromagnetism; this is because the atoms in a liquid change positions at an incredible rate.

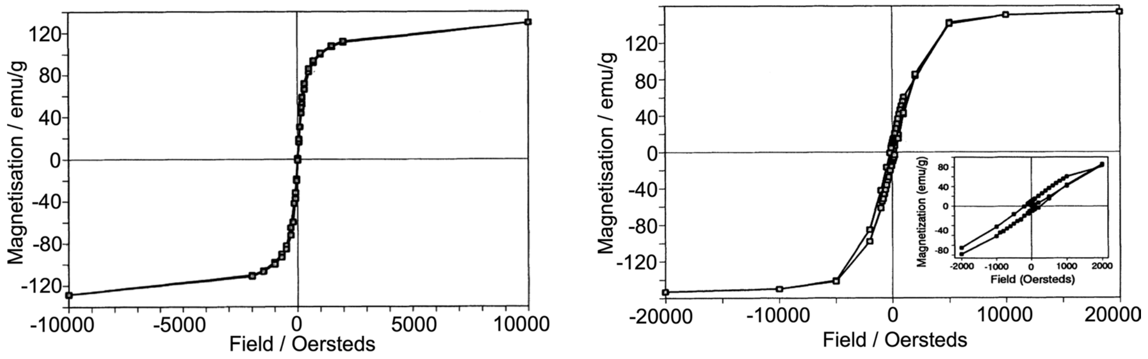

(a) (b)

Fig. 7 Hysteresis loops for amorphous iron (a) at 300 K. (b) At 9 K. One Tesla equals 10^4 Oersteds assuming a magnetic field in free space; 1 emu $g^{-1} \equiv 1$ A m^2 kg^{-1}. Reprinted with permission from Grinstaff et al. [26], copyright 1993 by the American Physical Society.

Table 1 Properties of pure, amorphous iron.

Enthalpy of crystallisation	15 kJ mol^{-1} at 580 K	[27]
Magnetic moment per atom (particles)	1.7 μ_B	[26, 27]
Magnetic moment per atom (films, 4.2 K)	1 → 1.5 μ_B	[28]
Electrical resistivity (films, 4.2 K)	1 → 1.5 μΩ m	[28]
Curie temperature (particles)	200 K	[27]
Packing fraction	0.66	[7]
Voronoi polyhedron (amorphous Fe)	$\overline{N}_{EF} = 5.12$, $\overline{N}_{Ve} = 23.7$, $\overline{N}_F = 13.8$, $\overline{N}_E = 35.5$	[7]
Wigner–Seitz polyhedron (α-Fe)	$\overline{N}_{EF} = 5.14$, $\overline{N}_{Ve} = 24$, $\overline{N}_F = 14$, $\overline{N}_E = 36$	[7]

The terms $\overline{N}_{EF}$, $\overline{N}_{Ve}$, $\overline{N}_F$ and $\overline{N}_E$ represent the average number of edges per face, number of vertices, number of faces and number of edge, for either a Voronoi polyhedron for the amorphous structure, or its equivalent for a regular structure, the Wigner–Seitz cell. Notice that $2\overline{N}_E/\overline{N}_F = \overline{N}_{EF}$ since each edge is shared between two faces

particles, the net magnetic moment of each particle can point in any direction, rather like paramagnetism, but since each ferromagnetic particle has very many coupled atomic moments, the phenomenon is known as superparamagnetism, illustrated in Fig. 8. The average magnetisation of this collection of particles sums to zero. When an external field is applied, the moments of the particles align to that, but the saturation magnetisation is less than found with the crystalline form, the discrepancy attributed to crystalline disorder and surface effects [41].[3]

Thin films of amorphous iron

Thin objects can have different properties than bulk samples. Just to set this into context, there are two special magnetic effects associated with crystalline thin films of iron [44, p.43,]. First, the magnetic moment per atom becomes especially large (3.1 μ_B) when compared with bulk iron (2.2 μ_B). Secondly, there exists a large magnetic anisotropy in thin epitaxial films of iron. The increase in the magnetic moment per atom is due to the smaller coordination number for atoms in a thin film. The atoms of the substrate used to produce the thin film do not contribute to the coordination number because there is a lack of hybridisation between the electronic states of the iron layer and the substrate [45, 46]. The *d*-bands in bulk ferromagnets are much broader than they would be for a single atom because of hybridisation between atoms. In reducing the number of nearest neighbours, the hybridisation is reduced so the bands

---

[3] Chattopadhyay and co-workers have reported superparamagnetic behaviour in grains of $ZnFe_2O_4$ nano-structured samples [42] and in $Fe_{73.5}CuNb_3Si_{13.5}B_9$ prepared by mechanical alloying [43]. It is also argued that in very small particles, such as the nano-magnets for use in memory storage devices, the appearance of the superparamagnetic state makes the device susceptible to thermal fluctuations because the magnetocrystalline energy is too small relative to the thermal energy kT [5].

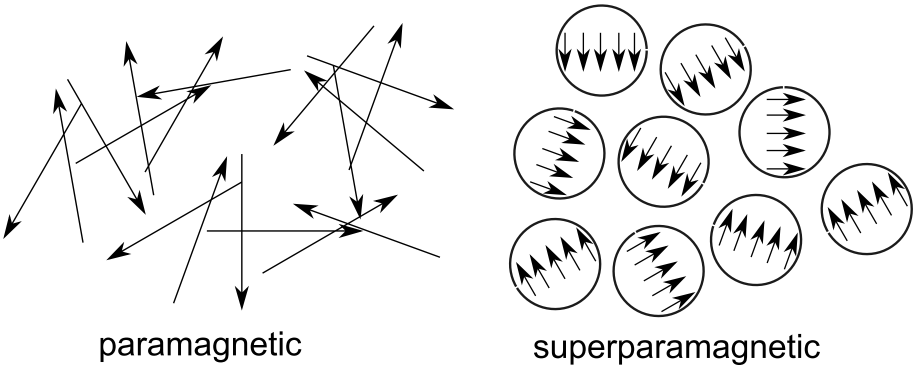

Figure 8 Illustration of the difference between paramagnetism where the individual magnetic moments are randomly aligned, and superparamagnetism where clusters of moments are randomly aligned in a suspension of nanoparticles.

become 'atom-like'. This squashing of the *d*-bands increases the density of states at the Fermi level and resolves the majority spin-up band from the minority spin-down band. A low-coordination atom therefore has more electrons in its majority spin-up band, and so a larger moment per atom. An isolated atom has the highest moment and the bulk material the lowest. Reducing the coordination makes the material less bulk-like and more single atom-like.

The magnetic anisotropy seen in thin films is a general feature found even in bulk iron where it is more readily magnetised along the ⟨100⟩ axis [47]. Anisotropy is caused by the coupling of the directions of the spin magnetic moments and orbital magnetic moments. For a thin film of iron, the net effect is often such that it causes the spins to align in a direction normal to its plane. Thin layers of iron separated by intervening layers of chalcogenides have been found to be highly anisotropic with the internal field perpendicular to the plane [48]. Such materials show a large change in resistance as the magnetic field is altered and could conceivably have applications in recording devices.

Thin film effects pervade in other materials. In recent work, Chattopadhyay and co-workers showed that manganese–telluride thin films prepared by exfoliating liquid exhibited huge magnetic saturation when compared with the bulk material at ambient temperature [49]. At the same time, the antiferromagnetic behaviour of bulk samples was replaced by paramagnetism in the thin film form. The Néel temperature shifted from 307 K to 290 K in the two-dimensional form, which is consistent with its paramagnetic behaviour at ambient temperature (≈ 300K).

Focusing now on iron, there are multiple ways of depositing thin films, one being the evaporation of iron onto a thick amorphous carbon substrate at a pressure of 8×10^{-3} Pa, with the thickness of the film increasing at $\approx 0.5\,\mathrm{nm\,s^{-1}}$ [50]. Each film was deposited as a circular disc of uniform thickness but tapering to zero at the edge. With the substrate at liquid helium temperature (4.2 K), the film evolves in an amorphous state but crystallises spontaneously at that temperature, by islands of amorphous material transforming suddenly into single crystals. This happened on reaching a critical film thickness which is 3.4 nm or 25 nm for deposited disc radii of 25 μm and 5 μm, respectively. This dependence on disc radius has its origins in the stress generated either by the crystallisation event that leads to densification, effectively of a constrained film, and possibly magnetostriction effects.

Only crystalline α-iron is obtained when deposited with a substrate temperature of 300 K, with a grain size that is much finer than obtained during the spontaneous crystallisation of the sample deposited at 4.2 K. It is possible that the larger grain size in the latter case is due to local heating during sudden crystallisation [50].

Sputtering has been used to produce structures that have alternating layers of iron and another element such as gadolinium and dysprosium [51, 52]. The iron when first deposited remains amorphous, but on reaching a certain thickness, the entire layer crystallises. It is suggested that this has to do with the misfit between iron and the dissimilar layers, which accumulates as its thickness increases, until the influence of the interface diminishes to the point where crystallisation sets in.

Summary

Pure iron is interesting—it occurs as a liquid, vapour, crystalline form (body-centred cubic, cubic close-packed, hexagonal close-packed, trigonal and tetragonal crystal structures) and has been produced as an amorphous solid. However, the amorphous state is not achieved easily, and when samples are successfully made, they are very small in size, either as small particles or as thin films. There is no application as yet, in spite of the good intentions of the opening paragraphs of many publications. The subject nevertheless is fascinating and has inspired considerable theoretical efforts ranging from the random physical arrangement of hard balls, to computational simulations that deal with many thousands of atoms. These simulations have rather nicely identified the conditions needed to produce pure iron in an amorphous state, disclosing the locations of atoms and images indicating the coexistence of the glassy and crystalline states under appropriate circumstances. There has even been a daring attempt to simulate the stress–strain curve in uniaxial compression of glassy iron to very large plastic strains, but there remain many unexplained features in the predicted behaviour.

Finally, it is a veritable pleasure to acknowledge Professor Kamanio Chattopadhyay, whose presence I have felt in both India and the UK. One of the nicest people I have had the privilege to meet and a brilliant scientist to boot.

Declarations

Conflict of interest The author declares that has no conflict of interest. The study is not funded by any grant.

References

[1] Chattopadhyay K, Ramachandrarao P (1976) Multiply twinned particles in an aluminium-nickel vapour deposit. J Cryst Growth 36:355–357

[2] Chattopadhyay K (2024) 'Private communication to H. K. D. H. Bhadeshia', : First paper published by Kamanio

[3] Chattopadhyay K, Ramachandrarao P (1974) The structure of a eutectic alloy solidified over a heat pipe. Scr Metall 8:1083–1087

[4] Chattopadhyay K, Ramachandrarao P, Lele S, Anantharaman T (1976) 'Crystal structure of a metastable aluminum-nickel phase obtained by splat cooling', In: Rapidly Quenched Metals. Massachusetts, USA: MIT Press, 157–161

[5] Tiwari K, Devi MM, Biswas K, Chattopadhyay K (2021) Phase transformation behavior in nanoalloys. Prog Mater Sci 121:100794

[6] Chattopadhyay K, Goswami R (1997) Melting and superheating of metals and alloys. Prog Mater Sci 42:287–300

[7] Yamamoto R, Doyama M (1979) The polyhedron and cavity analyses of a structural model of amorphous iron. J Phys F: Met Phys 9:617–627

[8] March NH (2009) Liquid metals, concepts and theory: Cambridge. Cambridge University Press, UK

[9] Pan S, Qin J, Wang W, Gu T (2011) Origin of splitting of the second peak in the pair-distribution function for metallic glasses. Phys Rev B 84:092201

[10] Bernal JD (1964) The Bakerian lecture, 1962. The structure of liquids. Proc R Soc Lond A 280:299–322

[11] Bennett CH (1972) Serially deposited amorphous aggregates of hard spheres. J Appl Phys 43:2727–2734

[12] Ichikawa T (1975) The assembly of hard spheres as a structure model of amorphous iron. Physica Status Solidi (a) 29:293–302

[13] Hermann H, Mattern N (1986) Analytic approach to the structure of amorphous iron-boron alloys. J Phys F: Met Phys 16:131–140

[14] Mo J, Liu H, Zhang Y, Wang M, Zhang L, Liu B, Yang W (2017) Effects of pressure on structure and mechanical property in monatomic metallic glass. J Non-Cryst Solids 464:1–4

[15] Mishima O, Calvert L, Whalley E (1985) An apparently first-order transition between two amorphous phases of ice induced by pressure. Nature 314:76–78

[16] Pandey K, Garg N, Shanavas K, Sharma SM, Sikka S (2011) Pressure induced crystallization in amorphous silicon. J Appl Phys 109:113511

[17] He D, Zhao Q, Wang W, Che R, Liu J, Luo X, Wang W (2002) Pressure-induced crystallization in a bulk amorphous zr-based alloy. J Non-Cryst Solids 297(1):84–90

[18] Liu H, Wang L, Xiao X, De Carlo F, Feng J, Mao H-K, Hemley RJ (2008) Anomalous high-pressure behavior of amorphous selenium from synchrotron X-ray diffraction and microtomography. Proc Natl Acad Sci 105:13229–13234

[19] Chang H, Kim D, Kim Y, Kim Y, Chattopadhyay K (2006) On the origin of nanocrystals in the shear band in a quasicrystal forming bulk metallic glass Ti40Zr29Cu9Ni8Be14. Scripta Mater 55:509–512

[20] Xu J, Xiang M, Dang B, Jian Z (2017) Relation of cooling rate, undercooling and structure for rapid solidification of iron melt. Comput Mater Sci 128:98–102

[21] Jian Z, Jie W, Jian Z (2001) Criterion for judging the homogeneous and heterogeneous nucleation. Metall and Mater Trans A 32:391–395

[22] Polizzi S, Antonangeli F, Piacentini M, De Crescenzi M (1984) Structural and electronic properties of laser irradiated pure iron. Solid State Commun 50:251–256

[23] Gu X, Poon SJ, Shiflet GJ (2007) Mechanical properties of iron-based bulk metallic glasses. J Mater Res 22:344–351

[24] Klement Jun W, Willens RH, Duwez P (1960) Non-crystalline structure in solidified gold-silicon alloys. Nature 187:869–870

[25] Suslick KS, Choe S-B, Cichowlas AA, Grinstaff MW (1991) Sonochemical synthesis of amorphous iron. Nature 353:414–416

[26] Grinstaff MW, Salamon MB, Suslick KS (1993) Magnetic properties of amorphous iron. Phys Rev B 48:269–274

[27] Chen Q, Sundman B (2001) Modeling of thermodynamic properties for bcc, fcc, liquid, and amorphous iron. J Phase Equilib 22:631–644

[28] Raeburn S, Aldridge R (1978) The Hall effect, resistivity and magnetic moment of amorphous and polycrystalline iron films. J Phys F: Met Phys 8:1917–1928

[29] Coey JM (2010) Magnetism and magnetic materials: Cambridge. Cambridge University Press, UK

[30] Lorenz R, Hafner J (1995) Noncollinear magnetic structures in amorphous iron and iron-based alloys. J Magn Magn Mater 139:209–227

[31] Liebs M, Fähnle M (1996) Amorphous iron revisited: an ab initio study. Phys Rev B 53:14012

[32] Bellissent R, Galli G, Grinstaff M, Migliardo P, Suslick K (1993) Neutron diffraction on amorphous iron powder. Phys Rev B 48:15797

[33] Falqui A, Loch D, Casu A (2020) In situ TEM crystallization of amorphous iron particles. Curr Comput-Aided Drug Des 10:10010041

[34] Cao X, Koltypin Y, Kataby G, Prozorov R, Gedanken A (1995) Controlling the particle size of amorphous iron nanoparticles. J Mater Res 10:2952–2957

[35] Barzola-Quiquia J, Osmic E, Häussler P (2021) The magnetic properties of amorphous Al_xFe_{100-x} alloys investigated by the atomic structure, magnetoresistance and anomalous hall effect. J Magn Magn Mater 526:167624

[36] Boswell P, Chadwick G (1976) The formation and crystallization of an amorphous phase in an iron-carbon alloy. J Mater Sci 11:2287–2296. https://doi.org/10.1007/BF00752093

[37] Hansen MF, Jönsson PE, Nordblad P, Svedlindh P (2002) Critical dynamics of an interacting magnetic nanoparticle system. J Phys: Condens Matter 14:4901–4914

[38] Van Wonterghem J, Mørup S, Charles SW, Wells S (1988) An investigation of the chemical reactions leading to the formation of ultrafine amorphous $Fe_{100-x}C_x$ alloy particles. J Colloid Interface Sci 121:558–563

[39] Miyatani R, Kobayashi Y, Yamada Y (2017) Thermal reaction of sonochemically prepared amorphous Fe/C. Hyperfine Interact 238:1–8

[40] Kazama N, Heiman N, White R (1978) Magnetic properties of amorphous FeC thin films. J Appl Phys 49:1706–1708

[41] Griffiths CH, O'Hara MP, Smith TW (1979) The structure, magnetic characterization, and oxidation of colloidal iron dispersions. J Appl Phys 50:7108–7115

[42] Chinnasamy C, Narayanasamy A, Ponpandian N, Chattopadhyay K, Guerault H, Greneche J (2000) Magnetic properties of nanostructured ferrimagnetic zinc ferrite. J Phys: Condens Matter 12:7795–7805

[43] Raja MM, Chattopadhyay K, Majumdar B, Narayanasamy A (2000) Structure and soft magnetic properties of finemet alloys. J Alloy Compd 297:199–205

[44] Bhadeshia HKDH (2021) Theory of Transformations in Steels: London. CRC Press, Taylor and Francis Group, UK

[45] Jonker BT, Walker KH, Kisker E, Prinz GA, Carbone C (1986) Spin-polarized photoemission study of epitaxial Fe(001) films on Ag(001). Phys Rev Lett 57:142–143

[46] Li C, Freeman AJ, Jansen HJF, Fu CL (1990) Magnetic anisotropy in low-dimensional ferromagnetic systems: Fe monolayers on Ag (001), Au(001) and Pd(001) substrates. Phys Rev B 42:5433–5422

[47] Haugan HJ, McCombe BD, Mattocks PG (2002) Structural and magnetic properties of thin epitaxial Fe films on (110) GaAs prepared by metalorganic chemical vapor deposition. J Magn Magn Mater 247:296–304

[48] Edelstein AS, Murday JS, Rath BB (1997) Challenges in nanomaterials design. Prog Mater Sci 42:5–21

[49] Gowda CC, Tromer R, Pandey P, Chandravanshi D, Chandra A, Chattopadhyay K, Galvao DS, Tiwary CS (2023)

Magnetic behavior of two-dimensional manganese telluride. 2D Materials 10:045006

[50] Bostanjoglo O, Giese W (1975) Stabilization of amorphous films by stress. Physica Status Solidi (a) 32:79–88

[51] Engl K, Brunner W, Zweck J (2002) Transition from amorphous Fe to polycrystalline body-centred-cubic Fe in Gd/Fe and Dy/Fe multilayered thin films. J Phys: Condens Matter 14:10033

[52] Landes J, Sauer C, Kabius B, Zinn W (1991) Critical thickness of the amorphous-nanocrystalline transition in Gd/Fe film structures. Phys Rev B 44:8342